Snowmelt-triggered debris flows in seasonal snowpacks

Benjamin Hatchett[1*], *Steven* Bacon[2], *W. Tyler* Brandt[3], *Anne* Heggli[1], and *Jeremy* Lancaster[4]

[1]Division of Atmospheric Sciences, Desert Research Institute, Reno, Nevada, USA
[2]Division of Earth and Ecosystem Sciences, Desert Research Institute, Reno, Nevada, USA
[3]Center for Western Weather and Water Extremes, Scripps Institution of Oceanography, La Jolla, California, USA
[4]California Geological Survey, Sacramento, California, USA

Abstract. Snowmelt-triggered debris flows commonly occur in mountains. On 14 June 2019, a debris flow occurred on a steep, east-facing slope composed of unconsolidated glacial and periglacial sediments in Yosemite National Park. Originating as a shallow landslide, ~1,300m^3 of ripe snow was instantaneously entrained into the debris flow carrying boulders, trees, and soil downslope. The forested area at the toe of the slope strained out debris leaving a muddy slurry to issue across Highway 120 during dewatering. We document this mass movement and assesses its initiation using local snowpack and meteorological data as well as a regional atmospheric reanalysis to examine synoptic conditions. A multiday warming trend and ripening of the snowpack occurred prior to the event as a 500 hPa ridge amplified over western North America leading to record warm 700 hPa temperatures. Anomalous temperatures and cloud cover prevented refreezing of the snowpack and accelerated its ripening with meltwater contributing to soil saturation. Similar conditions occurred during the catastrophic 1983 Slide Mountain debris flow, also hypothesized to be snowmelt initiated. With projected increases in heat waves, our findings can support natural hazard early warning systems in snow-dominated environments.

1 Introduction

Snowmelt-triggered debris flows occur in mountains worldwide with a range of impacts depending on downstream values at risk. Icy debris flows [1], pooling of snowmelt that ultimately induces failure [2], snowmelt-induced landslides [3], as well as rock and ice fall [4] can trigger debris flows, damaging downstream life and property. The typical initiation of debris flows results from pooling of snowmelt in persistent snowfields, leading to runoff-generated debris flows.

Ongoing warming of snow-dominated mountains will increase likelihoods of natural hazard occurrences relating to rapidly melting ice or snow [5]. Here, we aim to (1) document a rarely observed mass movement in California's seasonal snow zone during 2019, and (2) address the hypothesis that the 2019 event, and another in 1983, resulted from saturated soils following multi-day heat waves that contributed to snowpack ripening and melt with amplified melt rates resulting from high relative humidity, strong solar radiation, and downwelling longwave radiation all of which prevented snowpack refreezing.

In contrast to debris flows resulting from pooling beneath persistent snowfields, our study areas focus on seasonal snowpacks that undergo an annual cycle of accumulation and melt. By applying a multidisciplinary framework to analyse the geomorphic setting and outcome of the 2019 event, the synoptic and local scale atmospheric conditions preceding and during both 2019 and 1983 events, and the snowpack conditions associated with the 2019 event, our analysis can provide guidance for the development of improved early warning systems for natural hazards in mountain environments. As mountains become increasingly exposed to events that were infrequent or rare under cooler climate conditions, such systems can reduce impacts to life and property.

2 Geomorphic Setting and Site Description

The debris flow originated at approximately 3,148 m on a 40° east aspect in a nivation hollow beneath protalus ramparts along the Gaylor Peak Ridge at approximately 37.90180°N, -119.26402°W (Figure 1a). This slope is near the Tioga Pass Entrance Station to Yosemite National Park on Highway 120 (Figure 1b) and located near the middle of a 3.3 km long north-south trending ridge culminating with Gaylor Peak to the north.

The protalus ramparts above the slope are combinations of weathered and fractured Creteaceous granodiorite bedrock, gendarmes, and boulders. In the nivation hollow below the ramparts, the slope is composed of a jumble of clast-supported, poorly sorted glacial deposits with rounded talus and scree to fine grained silts. Along the upper slopes, soils are poorly developed but thickened with the transition into forested slopes halfway downslope. The slope transitions to an

* Corresponding author: benjamin.hatchett@dri.edu

© The Authors, published by EDP Sciences. This is an open access article distributed under the terms of the Creative Commons Attribution License 4.0 (https://creativecommons.org/licenses/by/4.0/).

alluvial fan before terminating in a flat, seasonally wet meadow (Figure 2a).

Sentinel satellite imagery from 2019 shows no vegetation in the torrent channel, consistent with its June activity, and indicates the small depositional environment in the meadow (Figure 2b). Figure 2b also demonstrates the likely scar (landslide source) from the most recent mass movement event and the three fingers of water-rich debris issued beyond the debris fan into the meadow. These fingers are consistent with the photograph taken on the day of the event (Figure 1d). The presence of the depositional fingers indicates the image was acquired after the event. Figures 1e-f show the location of the origin of the shallow landslide and subsequent snowpack collapse and entrainment.

Fig. 1. (a) Initial view of the debris flow event. (b) Study location in the Tioga Pass, California region with red dots showing the locations of surface meteorology and snowpack observations. (c) Several cyclists investigating the mud and debris as the road became impassable to vehicle and bicycle traffic. Active dewatering was occurring at this time. (d) Hyperconcentrated flow issuing out into Dana Meadows and incising into the snowpack. Note the deposition fingers in the center of the image. (e) and (f) Main scarp showing the characteristic glacially deposited, clast-supported, poorly sorted boulder- to silt-sized clasts, the flanks and crown of the snowpack collapse, head scarps of the shallow landslide, and rills incising the landslide rupture surface.

A digital elevation map provides additional evidence for mass movement and fluvial activity. The hillshade further reveals the presence of an approximately 2 m wide torrent channel terminating in a classic triangular debris fan (Figure 2c). The watershed contributing area, or accumulation area (Figure 2a), was calculated in CalTopo to be approximately 28,000 m^2. Above the road, the debris fan is estimated at 4,000 m^2. Including the area inundated across Dana Meadows (mapped via satellite imagery; Figure 2b), the total depositional area is estimated to be on the order of 4,000 m^2.

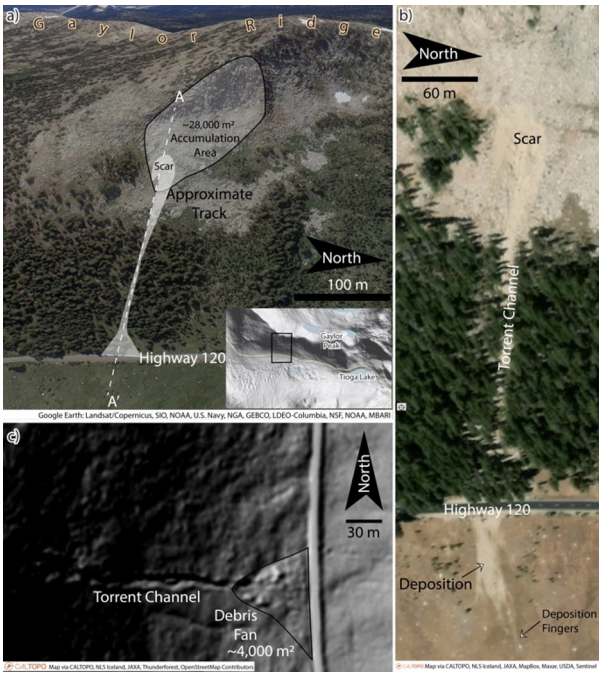

Fig. 2. (a) Oblique Google Earth image of the shallow landslide area on Gaylor Ridge with estimated watershed accumulation area, scar, torrent track, and debris fan. (b) Sentinel imagery provided by CalTopo showing the scar from the landslide's zone of depletion, the torrent channel, and the deposition into the debris fan above Highway 120 and into Dana Meadows (note depositional fingers photographed in Figure 1d). (c) Shaded relief image showing the torrent channel and debris fan.

3 Station and Meteorological Data

3.1 Station Data

Sub-hourly observations of temperature, precipitation, snow water equivalent, relative humidity, snow depth, and solar radiation were acquired from the Dana Meadows and Tuolumne Meadows California Cooperative Snow Survey Sensors via the California Data Exchange Center (CDEC; http://www.cdec.water.ca.gov) for the period spanning 12 am local time on 30 May 2019–12 pm 15 June 2019.

3.2 Meteorological Data Using Atmospheric Reanalysis Products

Daily averages (00Z) of 36 km horizontal resolution 700 hPa air temperature and 500 hPa geopotential height were acquired from the North American Regional Reanalysis (NARR) spanning the period 11-14 June 2019. The characteristic terrain height is near 3,200 m, thus the 700 hPa pressure surface in the NARR is an ideal model pressure level to assess conditions. 700 hPa is also a very commonly output pressure level from numerical weather prediction models, thus can be used to forecast free atmospheric conditions in the northern and central Sierra Nevada near and just above its crest elevation.

Anomalies of geopotential height and temperature were calculated by differencing the daily event values

from long term averages of the corresponding calendar days spanning 1981-2010. Daily rankings of temperatures were calculated by sorting each grid point in the NARR period of record (1979-2021) and identifying the rank of the date of interest.

4 Results

4.1 Heatwave precedes debris flow

Maximum temperatures at Dana Meadows exceeding 10°C started on 9 June and warmed through 11 June (18.3°C) before slowly cooling until the time of the event on the afternoon of 14 June (15°C; Figure 3a). The remaining analysis focuses on 11-14 June that covers the peak of the heatwave until the debris flow occurred.

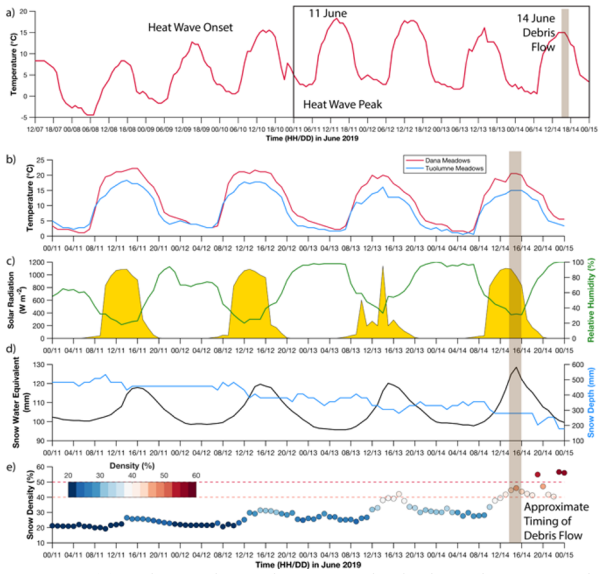

Fig. 3. (a) Timeseries of meteorological and snowpack conditions. a) Near-surface (2 m) temperatures at Dana Meadows spanning 1200 hrs 7 June-00 hrs 15 June (local time). (b) Near-surface (2 m) temperatures at Dana Meadows (red line) and Tuolumne Meadows (blue line), (c) solar radiation (filled gold areas) and relative humidity (green line) at Dana Meadows, (d) snow water equivalent (black line) and snow depth (blue line) at Dana Meadows, and (e) snow density (filled dots) spanning 1200 hrs 7 June-00 hrs 15 June (local time). The light brown vertical bar indicates the approximate timing of the debris flow, constrained by human observations.

Temperatures at Dana Meadows (2987 m) versus Tuolumne Meadows (2621 m) were consistently 3-5°C hotter during the peak hours of the day (Figure 3b). Both stations reached similar minimum temperatures with additional cooling prevented after atmospheric saturation achieved and latent heat released (interpreted from Dana Meadows relative humidity reaching 100%; Figure 3c). Minimum temperatures at both stations remained above 0°C throughout the period, with the last below-freezing minimum temperature on 9 June.

Generally clear skies are suggested by solar radiation, however greater cloud cover on 13 June and light high-level cloud cover on 14 June (Figure 3c) likely enhanced downwelling longwave radiation to the snow surface, potentially further enhancing melt rates as snow effectively absorbs longwave radiation.

4.2 Heat wave results from amplified 500 hPa ridge and record 700 hPa temperatures

Midtropospheric (500hPa) height anomalies indicate the presence of an amplified ridge over western North America during 11-14 June (Figure 4). Amplified ridging favors downward vertical motions and anomalously positive temperatures in the lower troposphere and at the Earth's surface. Mountain-top temperature anomalies in the free atmosphere (700 hPa) over the region during 11-14 June ranged from +3 to +8°C, with the hottest anomalies occurring on 11 June (Figure 4a). Above-freezing 700 hPa temperatures, cloud cover, and high relative humidities prevented nocturnal snowpack refreezing–indicated by the increase in snowpack density (Figure 3e)–leading to continuous liquid water input to the soil surface.

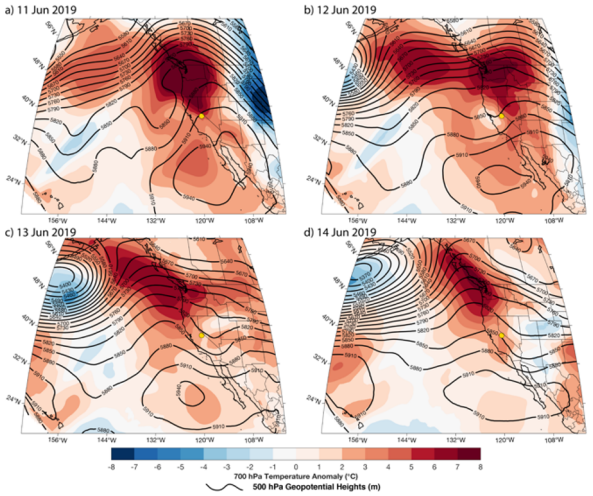

Fig. 4. 700 hPa temperature anomalies (filled contours) and 500 hPa geopotential heights (black contours) for a) 11 June 2019, a) 12 June 2019, a) 13 June 2019, and d) 14 June 2019.

Rankings of 700 hPa temperatures indicate the peak day of the heatwave (11 June 2019) was the hottest in the NARR period of record (Figure 5). Widespread top (highest since 1979) rankings occur throughout eastern North Pacific and western North America encompassing an area from 140°W to 110°W and from (20°N) to 56°N.

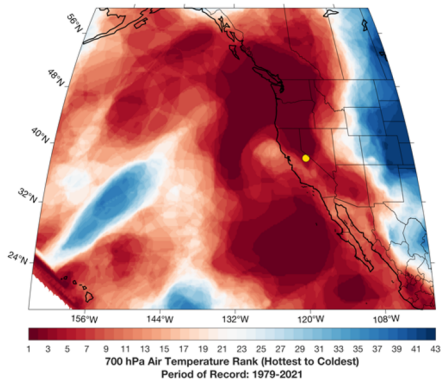

Fig. 5. Rankings of 11 June 2019 (hottest date of June 2019 heatwave) 700 hPa temperatures with respect to the NARR period of record (1979-2021). Gold dot indicates Tioga Pass.

5 Application to 30 May 1983 Slide Mountain Debris Flow

The 30 May 1983 Slide Mountain landslide and subsequent debris flow followed a near-record snowfall year [3]. The slope failure initiated near the summit of Slide Mountain, Nevada (eastern Sierra Nevada) and entrained snow on the southeastern aspect of the upper slopes. Water was also entrained as material and debris flowed downslope into Upper Price Lake. The resulting slurry (1.07×10^6 m^3) flowed 4 kilometers down Ophir Creek and issued onto an alluvial fan proximal to Washoe Lake, inundating Highway 395 and multiple homes constructed on the alluvial fan, killing one.

Applying a similar analysis to the 2019 event, but using mean temperatures spanning the 11-14 June period (Figure 6a), we find anomalous positive 700 hPa temperatures throughout the 27-30 May 1983 period (Figure 6b). Temperature anomalies during the May 1983 event were of similar magnitudes compared to June 2019 (exceeding +8°C above the mean), but were more widespread across western North America. 700 hPa temperature rankings during the May 1983 Slide Mountain debris flow were also among the hottest in the NARR period of record (Figure 7).

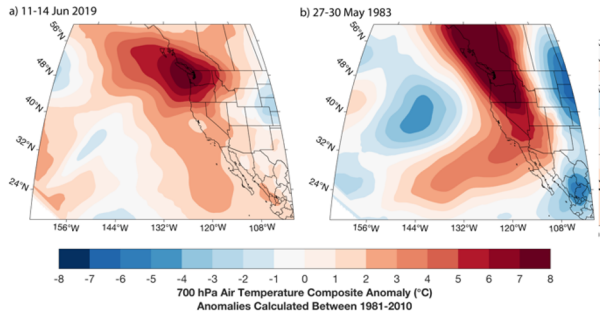

Fig. 6. Maximum mean 700 hPa temperature anomaly rankings during (a) 11-14 June 2019 and (b) 27-30 May 1983.

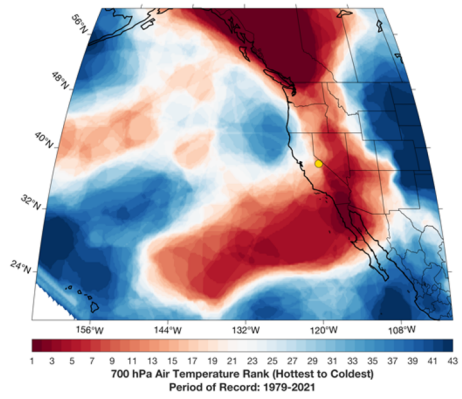

Fig. 7. As in Figure 5 but for 30 May 1983 Slide Mountain debris flow (hottest date of May 1983 heatwave shown).

6 Discussion

We documented a unique snowmelt-triggered mass movement during June 2019 in the Sierra Nevada (USA) that resulted from a sequence of extreme weather events in a high mountain environment. This sequence included late spring heat waves with record-to-near record multiday temperatures and high solar radiation following anomalously snowy winters. Anomalously warm temperatures and solar radiation led to snowmelt that likely increased soil moistures and soil pore pressures and induced shallow landslide failure. Because remnant seasonal snow remained, ripe (near 0°C) snow was entrained and melted, creating a slurry that flowed downslope and issued upon infrastructure built along an alluvial fan, leading to road closures and minor damage. A similar sequence occurred during the much larger and more damaging 1983 Slide Mountain debris flow, providing confidence in our identified sequence of events and supporting our hypothesis.

While snowmelt-triggered debris flows are relatively rare in non-glaciated mountains, we expect warming temperatures (higher maximum and fewer minimum temperatures below freezing), increased precipitation variability, and more frequent heat waves to produce an increase in the likelihood of these events. As *in situ* networks providing observations of relevant parameters such as snowpack temperature and density, air temperature, soil moisture, and solar radiation are uncommon in many mountain areas worldwide, we suggest applying atmospheric reanalysis products as well as satellite-based products of solar radiation and snow albedo to develop predictive tools. These tools can then incorporate weather forecasts as input to early warning systems.

Solar radiation is a key driver of snowmelt [6] and may provide explanatory power for events that did not experience anomalous high temperatures. Reductions in snow albedo from snow grain growth and deposition of light absorbing aerosols (e.g., dust and black carbon) multiply the effects of anomalous solar radiation in elevating snowmelt rates [7]. Forensic case studies of unique events, such as presented here, can be used to develop snowmelt-induced hazard early warning tools for application in mountains with otherwise limited observational networks.

References

1. D.F. Ritter, R.C. Kochel, R. Miller, Process Geomorphology (McGraw Hill, Boston, 2002)
2. D. Rickenmann, M. Zimmermann, Geomorphol., **2(8)**, 175-189 (1993)
3. R.J. Watters, A landslide induced waterflood-debris flow, Bull. Int. Assoc. Engin. Geol., **28**, 177-182 (1983)
4. D.H. Shugar et al., A massive rock and ice avalanche caused the 2021 disaster at Chamoli, Indian Himalaya, Science, 373, 300-306 (2021)
5. D. Marks, J. Dozier, Climate and energy exchange at the snow surface in the Alpine Region of the Sierra Nevada: 2. Snow cover energy balance, Wat. Res. Resear., **28(11)**, 3043-3054 (1992)
6. A.L. Koshkin, B.J. Hatchett, A.W. Nolin, Wildfire impacts on western United States snowpacks, Front. Water, in press (2022).